NANO MICRO small
www.small-journal.com

Alpha Lead Oxide (α-PbO): A New 2D Material with Visible Light Sensitivity

Prashant Kumar, Jing Liu, Pranay Ranjan, Yaowu Hu, Sharma SRKC Yamijala, Swapan K. Pati, Joseph Irudayaraj, and Gary J. Cheng**

Even though transition metal dichalcogenides (TMDCs) are deemed to be novel photonic and optoelectronic 2D materials, the visible band gap being often limited to monolayer, hampers their potential in niche applications due to fabrication challenges. Uncontrollable defects and degraded functionalities at elevated temperature and under extreme environments further restrict their prospects. To address such limitations, the discovery of a new 2D material, α-PbO is reported. Micromechanical as well as sonochemical exfoliation of 2D atomic sheets of α-PbO are demonstrated and its optical behavior is investigated. Spectroscopic investigations indicate layer dependent band gaps. In particular, even multilayered PbO sheets exhibit visible band gap > 2 eV (direct) which is rare among semiconducting 2D materials. The emission lifetime of multilayer PbO atomic sheets is 7 ns (dim light) as compared to the monolayer which gives 2.5 ns lifetime and an intense light. Density functional theory calculations of layer dependent band structure of α-PbO matches well with experimental results. Experimental findings suggest that PbO atomic sheets exhibit hydrophobic nature, thermal robustness, microwave stability, anti-corrosive behaviour and acid resistance. This new low-cost, abundant and robust 2D material is expected to find many applications in the fields of electronics, optoelectronics, sensors, photocatalysis and energy storage.

Graphene has emerged as one of the widely used nanomaterials due to its novel attributes and broad range of applications.[1–5] Since defects deteriorate electronic mobility, approaches for green synthesis are being highly sought to address such concerns.[6] However, single-layered pure graphene lacks electronic band gap which prevents it from being a replacement for silicon in electronic circuits. Graphene in the nanoribbon form do have a finite band gap and therefore, attaining defect-free graphene nanoribbons is of great interest.[7,8] While graphene has left a wonderful legacy, novel 2D materials beyond graphene and their heterostructures are therefore being conceptualized.[9] Transition metal dichalcogenides (TMDCs), such as MoS_2, have evolved well in time.[10–16] The electronic band gap of monolayer MoS_2 is ≈1.8 eV and exhibits photoluminescence (PL) peaks at ≈1.85 and at 1.98 eV. While bulk MoS_2 has indirect band gap; at the

Dr. P. Kumar, Dr. J. Liu, Dr. Y. Hu, Prof. J. Irudayaraj, Prof. G. J. Cheng
Birck Nanotechnology Centre
Purdue University
West Lafayette, IN 47907, USA
E-mail: josephi@purdue.edu; gjcheng@purdue.edu
Dr. P. Kumar, Dr. Y. Hu, Prof. G. J. Cheng
School of Industrial Engineering
Purdue University
West Lafayette, IN 47907, USA
Dr. P. Kumar, P. Ranjan
Department of Physics
Indian Institute of Technology
Bihta Campus, Patna 801103, India
Dr. J. Liu, Prof. J. Irudayaraj
Bindley Bioscience Centre
Purdue University
West Lafayette, IN 47907, USA
Dr. J. Liu, Prof. J. Irudayaraj
Agricultural & Biological Engineering
Purdue University
West Lafayette, IN 47907, USA
Dr. J. Liu
Department of Physics
School of Science
Indiana University-Purdue University
IN 46202, USA
Dr. Y. Hu, Prof. G. J. Cheng
School of Mechanical Engineering
Purdue University
West Lafayette, IN 47907, USA
Dr. Y. Hu
Department of Mechanical and aerospace Engineering
University of Buffalo
Buffalo, NY 14260, USA
Dr. S. SRKC Yamijala
Chemistry and Physics of Materials Unit
Jawaharlal Nehru Centre for Advanced Scientific Research
Bangalore 560064, India
Dr. S. SRKC Yamijala
Department of Chemistry
University of Rochester
Rochester, NY 14620, USA
Prof. S. K. Pati
Theoretical Sciences Unit
Jawaharlal Nehru Centre for Advanced Scientific Research
Bangalore 560064, India
Prof. J. Irudayaraj
University of Illinois at Urbana-Champaign
Urbana, IL 61820, USA

DOI: 10.1002/smll.201703346

monolayer, it develops a direct gap. Monolayer MoS_2 does give PL signal, while for multilayers, the signal is insignificant. Fabrication of large-area monolayer MoS_2 has been a challenge by micromechanical transfer process. Chemical vapor deposition of MoS_2 has not yet been developed till date to the level of commercialization. Other metal dichalcogenides have already been explored.[17,18] Strategies to realize optoelectronic sensing and photovoltaics operating in the visible range employing 2D materials are presently being explored due to high mobility of 2D materials. Adequate straining of MoS_2 atomic sheets,[19] fabrication of artificial 2D crystals by stacking various metal dichalcogenides, or graphene are some of the strategies presently being examined in this regard.[20–22]

Even though multipronged efforts are proposed, attaining such unique set of attributes from one material or a hybrid material is a challenging task. Therefore, one of the approaches to resolve such issues is to explore new 2D materials with visible band gap. Practical realization of visible range optoelectronic devices needs visible band gap even with higher number of layers, so that fabrication becomes easier. At the same time, signal to noise ratio should be significant so that the signal from external stimuli can unambiguously be recognized. Among various feasibilities, lead oxide (PbO) 2D sheets have been recognized as one of the most useful materials for optoelectronic sensing in the visible range.[23–25] Desirable attributes of PbO include: (a) good radiation absorbing property (due to the high atomic number and stability of Pb), (b) high resistivity to prevent leakage at extreme bias (necessary for efficient charge collection), and (c) abundant availability in nature. In addition, PbO has been hinted to be an ideal radiation detector.[26] In a nutshell, for applications with a visible excitation, PbO would be a suitable material for applications including photovoltaics, optoelectronic molecular sensing, and photocatalysis. There is, however, a dearth of systematic experimental evaluation on the optical characteristics of PbO at the atomic scale. The first among such studies would be band gap evaluation as one approaches atomic scale thicknesses. Such evaluation would not only establish PbO as a new 2D optical/optoelectronic material, it would also open opportunities for future exciting applications. Thus, there is a need to investigate 2D PbO sheets, especially its properties such as band gap as a function of the number of layers.

In this study, α-PbO 2D atomic sheets were attained by two different strategies namely micromechanical transfer of sheets to the substrates and sonochemical exfoliation synthesis. While micromechanical transfer yields high-quality pure atomic sheets, sonochemical synthesis seems to have potential for large-area applications of PbO. Optical microscopy, atomic force microscopy (AFM), and electron microscopy (field emission scanning electron microscopy (FESEM) and transmission electron microscopy (TEM)) were employed to demonstrate the successful transfer of 2D atomic sheets of α-PbO. X-ray diffraction (XRD), Raman spectroscopy, and X-ray photoelectron spectroscopy, along with atomic images in high resolution transmission electron microscopy (HRTEM) and selected area electron diffraction (SAED) were used to confirm their structural quality. Optical microscopy/spectroscopy as well as photoluminescence imaging/spectroscopy was utilized to investigate their optical excitonic behavior. Fluorescence lifetime measurements were carried out on PbO atomic sheets to explore excitonic time scale. Density functional theory (DFT) band structure calculations were utilized to determine layer-dependent band structure of α-PbO. While thermal, acid, and microwave resistance of this new 2D material was explored; its anticorrosive nature was examined. Wettability behavior of PbO sheets has also been investigated.

Most of the semiconducting 2D materials exhibit significant emission in the visible range only at the monolayer thickness. Micromechanical exfoliation yields few layered atomic sheets of MoS_2 (see optical and SEM images in Figure S1, Supporting Information). Dark-field optical imaging and PL imaging along with PL spectroscopy shows the visible range band gap of MoS_2 (Figure S2, Supporting Information). It should be noted that while a PL peak is observed centered around 670 nm for eight layers, three-layered PbO sheet exhibits PL peak at 655 nm. Even DFT band structure calculation carried out on 1–8-layered atomic sheets of MoS_2 proves that band gap increases when layers are cut down and direct band gap in the visible range is achieved only at the thickness of one layer (see Figure S3, Supporting Information). PbO with direct band gap of 2.5 eV even in its bulk form itself provides a magnificent platform for visible range optoelectronic and photovoltaic devices and sensors since this avoids fabrication of monolayers as has been the case with other metal dichalcogenides.[23–25]

Crystal structure of α-PbO at the atomic scale is shown in **Figure 1**a which clearly shows individual sheets which are bound by week van der Waals interactions. The layered nature of α-PbO would allow for the exfoliation of its atomic sheets. The equilibrium distance measured in the out of plane direction (*z*-direction), i.e., *c* is 5.023 Å and it has *P*4/*nmm* space group.[27,28] Apart from the electronic band gap, electron mobility is of crucial importance which determines how fast the device would respond to external stimuli. Effective mass of holes for monolayer PbO atomic sheet is ≈83 times than that of electrons. In contrast to its bulk counterpart, holes are only 6 times heavier than electrons.[29] In the case of PbO, delocalization of electron density in the conduction band (see Figure 1b) and heavy localization at Γ-point on oxygen (2p electrons) just at the top of the valence band (see Figure 1b) makes it a unique material.[27] Since holes become almost stagnant compared to electrons in the PbO monolayer, electronic conduction is primarily due to electrons and not due to holes and therefore, the PbO monolayer should exhibit n-type conduction. PbO atomic sheets have previously been used in X-ray detectors. These facts clearly positions PbO as an excellent material in the visible active optoelectronics. Figure S4 (Supporting Information) summarizes the crystal structures and band gaps of various 2D materials (visible range is highlighted in a color bar). Band structure calculated by DFT for atomic sheets of MoS_2 (Figure S3, Supporting Information) and α-PbO (Figure 1c). Trends in direct band gap at Γ-point with variation in the number of layers are shown in Figure 1d. Indirect band gap is shown for comparison. It can be observed that direct band gap at Γ-point increases from 2 eV (for eight layers) to 2.44 eV (for one layer). Similarly, indirect band gap increases from 1.45 eV (for eight layers) to 2.48 eV (for one layer). Based on direct band structure calculations, eight-layered PbO sheets which behave in many ways as its bulk counterpart should thus be red absorbing,

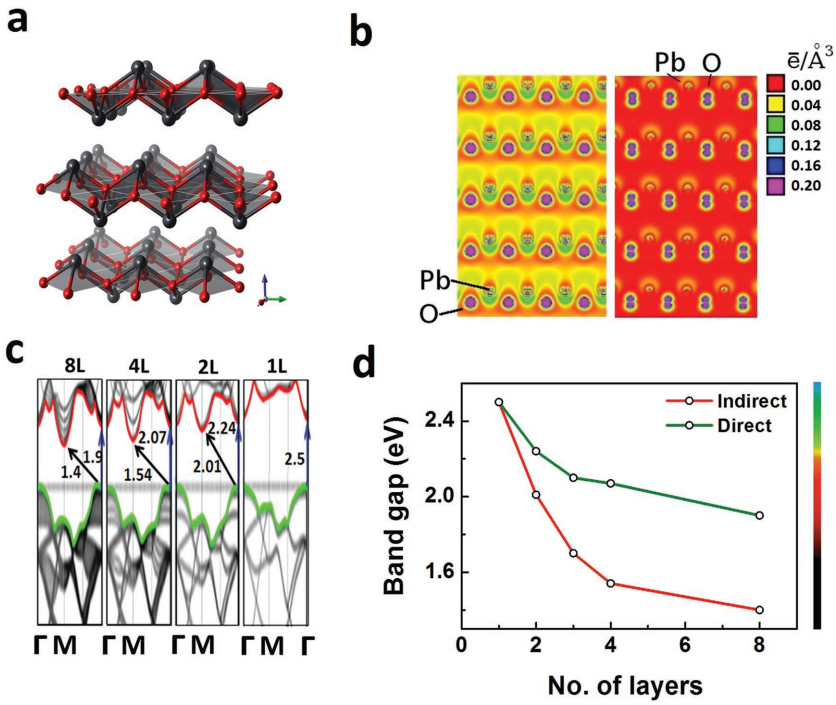

Figure 1. a) Schematic representation showing atomic bonding in α-PbO 2D crystal, b) the electron density map plotted with XcrySDen for bulk α-PbO for the conduction band (EC + 0.5 eV); and the valence band (EV –0.5 eV).[27] c) Band structure for 2D atomic sheets (calculated by DFT) of PbO and d) variation of direct and indirect band gaps with the number of layers.

while monolayers of PbO should be green absorbing. At all thicknesses down to monolayer, PbO has direct and indirect band gap in the visible range and is supposed to behave as a semiconductor. Even monolayers by themselves would be absorbing green light and that is very rare among atomic monolayers of known semiconductors.

FESEM image for 30-, 8-, and few layered α-PbO sheets are shown in **Figure 2**a–c, respectively. FESEM image in Figure 2c shows that few layers of α-PbO where one can vividly see transparent atomic sheets stacked on other. The number of layers is measured by the AFM line profile through the edge of the sheets. At the bottom, three layers and single layer α-PbO sheet veils it on the top and thus in common area, it is four atomic-layered sheet. In our case, sheets have been exfoliated by two approaches namely micromechanical exfoliation as well as by sonochemical exfoliation. Raman spectrum of micromechanically exfoliated few layered PbO atomic sheet is shown in Figure 2d, which confirms its chemical identity. Raman peaks at 80, 150, and 331 cm^{-1} corresponding to the *E*g, *A*1g, and *B*1g modes have been observed, which closely matches with the literature.[30] For PbO, interlayer interaction energy is just 0.016 eV per atom which is higher for graphene and MoS_2 and therefore they exhibit strong dependence on the number of layers. Thus, exfoliation of PbO atomic sheets would be easier than other 2D materials. AFM image of α-PbO atomic sheets shown in Figure 2e confirms the sheet-like structures. Line profile shown in Figure 2f reveals a thickness of 4 nm. Line profile being nonuniform at the top and the dip of 0.7 nm shows that on the top surface one layer is present which could not cover the whole area of the sheet. This demonstrates successful exfoliation and transfer of α-PbO 2D sheets. Transmission electron microscope (TEM) image shown in Figure 2g shows several electron-transparent atomic sheets whose lateral size ranges between 50 nm to more than a micrometer. Some sheets are triangular and some are polygonal in shape. However, all of these have smooth edges. SAED pattern shown in the Figure 2h confirms high level of chemical purity in terms of crystalline order. HRTEM image in Figure 2i reveals that atoms are well ordered. Yellow colored circles marked in Figure 2i confirm that atomic distances are same and the measured interplanar distance in HRTEM is 0.266 nm.

Characteristic X-ray diffraction peaks of α-PbO sheets (shown in **Figure 3**a) were observed. Peak at 35.6° represents [002] crystallographic plane of lead oxide. Further, all the peaks present matches well with ICSD-94333 which belong to group *P*4/*nmm*. The XRD patterns attained for our samples have further been matched with ICSD-60135 (Pbcm)[31] to confirm that β-PbO phase is not present in the material. To explore the actual valency of lead oxide in the present case, we investigated through X-ray photoelectron spectroscopy (XPS). Full range XPS spectrum of PbO is shown in Figure 3b where binding energies corresponding to different core level of Pb, O, and C have been marked. One of the phenomena observed is charging of the sample found to be more pronounced due to atmospheric exposure and its presence can be seen in the form of weak C-1s peak compared to Pb-4f. Figure 3c shows oxygen O-1s spectrum. It consists of an intense peak at ≈530 eV and a shoulder at low binding energy at ≈532 eV. Further, the core level spectrum of 3d, 4f, and 5d have been represented in Figure 3d–f, respectively. XPS peaks for Pb-$5d_{3/2}$, Pb-$4f_{5/2}$, and Pb-$4f_{7/2}$ orbitals have exactly matched with the literature[32] for PbO in contrast to other possible oxides, such as PbO_2 and Pb_3O_4. Most often, due to the environmental exposure (e.g., adsorption of O_2 or H_2O, etc.); valency of oxygen is influenced which would alter O-1s energy levels (mildly though) as observed in the present case as well.

To explore visible light sensitivity of PbO, spectroscopy was utilized. However, when these sheets are attained using scotch tape technique or even other techniques, signals would comprise of contributions from sheets with varying thicknesses, which may be misleading with respect to layer-dependent behavior. Therefore, scattering spectroscopy was used to probe one sheet at a time. This we believe will reveal the optical characteristics relating to its band gap. Bright field optical image of 30 layers of α-PbO sheets is as shown in **Figure 4**a and dark-field images are shown in Figure 4b. While, bright reddish yellow color of 30-layered sheets in the bright image appears, dark-field image shows scattering at the edges only. Hyperspectral dark field imaging is known for optical clearing.[33]

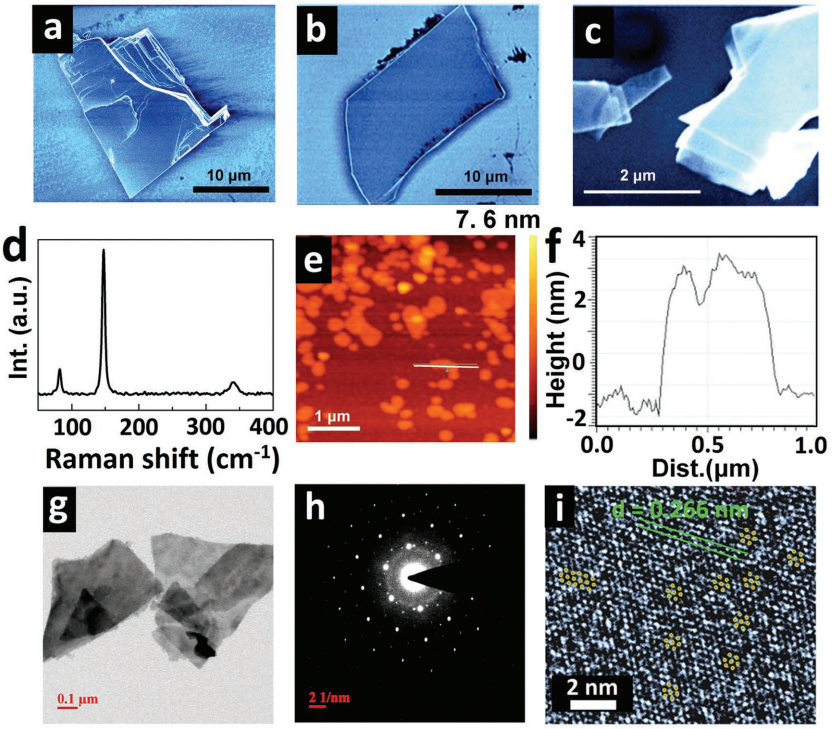

Figure 2. FESEM images of PbO atomic sheets with a) 30 layers, b) 8 layers, c) few layers, d) typical Raman spectrum of few layered α-PbO sheet, e) AFM image of 8 layer α-PbO atomic sheets, and f) line profile of one of the sheets in (e). g) TEM image, h) SAED of PbO sheets in TEM images shown in (h). i) HRTEM image with atoms marked for clarity.

However, scattering is very strong. Dark-field images for five and three layers are shown in Figure 4c,d, respectively. While five-layered sheets exhibit greenish scattering, three-layered sheets exhibited reddish scattering. For the quantification of such distinguished optical behavior, optical scattering spectra were recorded for five-layered sheets and three-layered sheets separately as shown in Figure 4e,f, respectively. Distinguishable scattering spectra are attained, one with the peak in the red region and the other in the green region. Results clearly imply that the red light is being absorbed by a five-layered sheet, while green light is being absorbed by the three-layered sheet, indicating a distinct layer-dependent optical behavior. Such behavior has been demonstrated for a variety of 2D materials. PbO material as such was never exfoliated and its optical characteristics reported in this study are the first evaluation of this new 2D material.

Absorption and emission characteristics are often different. Photoluminescence peaks are often observed at larger wavelengths compared to excitation wavelengths. This mostly happens since part of the excitation energy is being lost in heating mainly due to lattice defects. In our approach, to better understand the effect of visible light, especially on wavelength selectivity, photoluminescence spectroscopy experiments were carried out with various excitations. Luminescence images were obtained, while atomic sheets are being optically excited. Photoluminescence spectra for 3, 5, and 30-layered α-PbO atomic sheets with 488 nm excitation are shown in Figure 4g–I, respectively. The PL spectra have peaks at 675, 635, and 570 nm, respectively for 30, 5, and 3 layers. The corresponding band gap values (neglecting any energy loss) recorded were 1.83, 1.94, and 2.16 eV, respectively for 30, 5, and 3 layers, respectively. These results prove that as one reduces the number of layers, band gaps do increase in a substantial manner for PbO. Side and top views of the structures

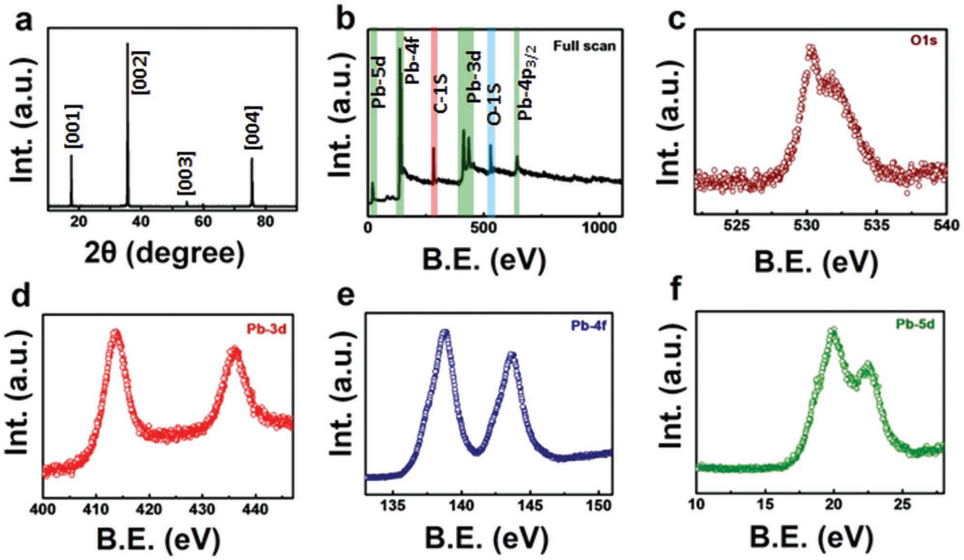

Figure 3. a) X-ray diffraction pattern of α-PbO sheets, b) full scan XPS spectrum of PbO sheet, XPS spectra for PbO sheet corresponding to c) O-1s, d) Pb-5d, e) Pb-4f, and f) Pb-3d.

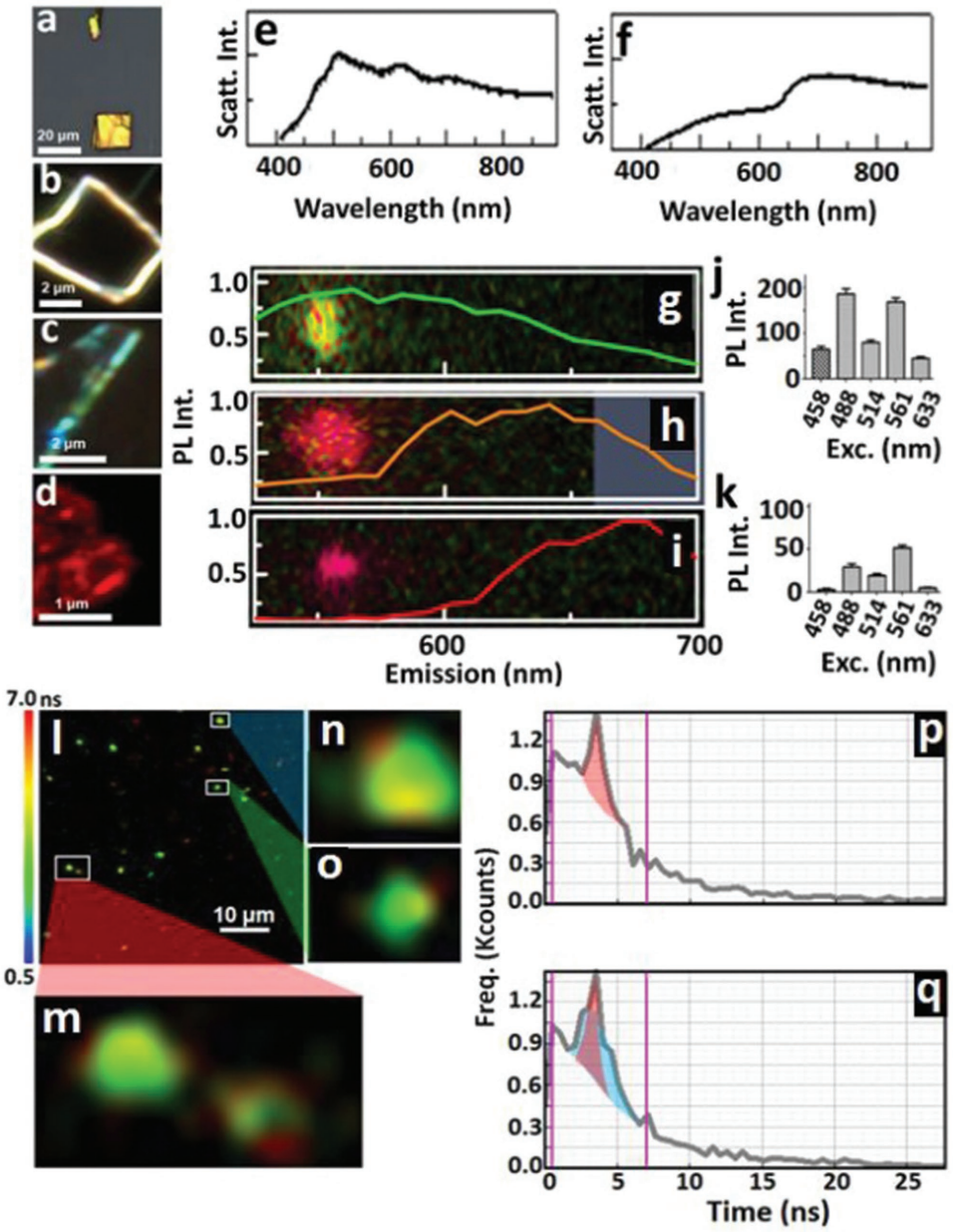

Figure 4. Optical image of α-PbO sheets of a) 30 layers (bulk); bright field, b) 30 layers (bulk); dark field, c) 5 layers; dark field and d) 3 layers; dark field. Optical scattering spectra in (e) and (f) correspond to (c) and (d). Photoluminescence spectra and images (in insets) for α-PbO atomic sheets with g) 3 layers, h) 5 layers, and i) 30 layers. Photoluminescence emission intensity versus excitation wavelength histograms for α-PbO atomic sheets with j) 3 layers and k) 30 layers. l) Lifetime imaging of PbO atomic sheets transferred on SiO2 substrate. (m), (n), and (o) are zoomed in images. (p) and (q) are time-resolved spectra for PbO sheets at two different spots.

of PbO used for band structure calculations are shown in Figure S5 (Supporting Information). Band structures for different "*n*" values for n-layered PbO sheets are shown in Figure S6 (Supporting Information). The experimental band gaps of 2.16 and 1.94 eV for three and five layers matches well with the direct band gaps calculated for PbO which is 2.073 and 1.9 eV, respectively. Based on our experiments, we expect PL peak for the monolayer to be even higher than 2.16 eV. The PL results obtained matches well with the optical scattering spectroscopy and with band structure calculations as well. Photoluminescence images attained with 488 nm excitation are shown in the inset of the spectra. When determining wavelength sensitivity of materials, excitation spectra are quite useful. In our system, we could attain histograms plotted for photoluminescence emission intensity versus excitation wavelength for 3- and 30-layered α-PbO atomic sheets as shown in Figure 4j,k, respectively. For a 30-layer sheet, maximum PL intensity was recorded at the excitation wavelength of 561 nm, and the emission was poor for 488 nm and almost negligible for 458 nm excitation. For a 3-layer sheet, however, maximum

emission was recorded at 488 nm excitation, while the 458 nm excitation gave rise to significant emission. Such excitation-specific emission measurements reveal a profound layer dependence of the optical excitation and emission. Emission peaks of 1–10 layers in the green to red visible range being very strong (high quantum yield) is of significance for visible range excitonics and related applications.

Fluorescence lifetime measurements carried out on PbO sheets reveal that the lifetime extended up to 7 ns (see Figure 4). Figure 4m–o is zoomed-in version of specific areas in Figure 4l. It is apparent from Figure 4l that the number of atomic layers in the sheets determines the lifetime. While monolayers or bilayers give more intense PL signal with smaller lifetime (red-shaded peaks in 4p,q). In the lifetime image, green spots represent such monolayers. Observation of lower lifetime for thinner layers (monolayers) is possibly due to the surface recombination limited for semiconducting atomic sheets.[34] In contrast, multilayers of PbO emit less intense light with prolonged lifetime (red color patches in lifetime images and peak with long tail in the spectra shown in Figure 4q). Time-resolved measurements hint at two distinguishable lifetimes for areas where there is a sharp contrast in the number of layers (see Figure 4q) and single lifetime in the areas where the number of layer is the same over an area of measurement (see Figure 4p). Our results imply that, in such materials where there are patches of multilayers on a large area of monolayers, there may be two channels for relaxation to occur. Defects formed in quantum dots primarily are detrimental to fluorescence lifetime.[35] Exciton lifetime is crucial as they determine whether these materials can be used in applications concerning excitonics or otherwise and therefore, relaxation mechanisms in 2D materials are presently being studied.[36–39] Photoluminescence decay in the range between 1.5 and 2.5 ns has been reported recently in the WSe_2 atomic sheets.[38] Early decay in polarization occurs due to intervalley relaxation or spin relaxation and this limits the exciton lifetime in MoS_2 sheets to 4–5 ps.[39] Thus, emission performance of PbO atomic sheets is appreciable and better than many other quantum dots. This is of significance since quantum dots are not chemically stable under elevated temperature/air/moist environment and in contrast PbO atomic sheets are robust.

Micromechanical exfoliation does have its own limitations, i.e., (a) difficulty in getting large-area monolayers, (b) nonuniformity of the number of layers, and (c) scalability of the method. To overcome such limitations and to demonstrate first few engineering applications of PbO atomic sheets, we have carried out sonochemical synthesis of PbO sheets. Starting material for the synthesis of PbO atomic sheets was already sheet-like naturally occurring α-PbO (see optical image in **Figure 5**a). Figure 5b shows the schematic representation of the sonochemical synthesis which usually results in synthesis of 1–10 layers and suitable centrifugation can be employed to achieve monolayer, bilayer, trilayer, etc. Solvent–material interaction plays a crucial role in determining the dispersion quality and their collective response to ultrasound. Such observation has already been made for other 2D materials including graphene, MoS_2, and new optically sensitive phosphorene.[40] We have, therefore, used di-methyl formamide (DMF) and water for sonication. Very tiny sheets were attained when DMF was used as a solvent (see TEM image

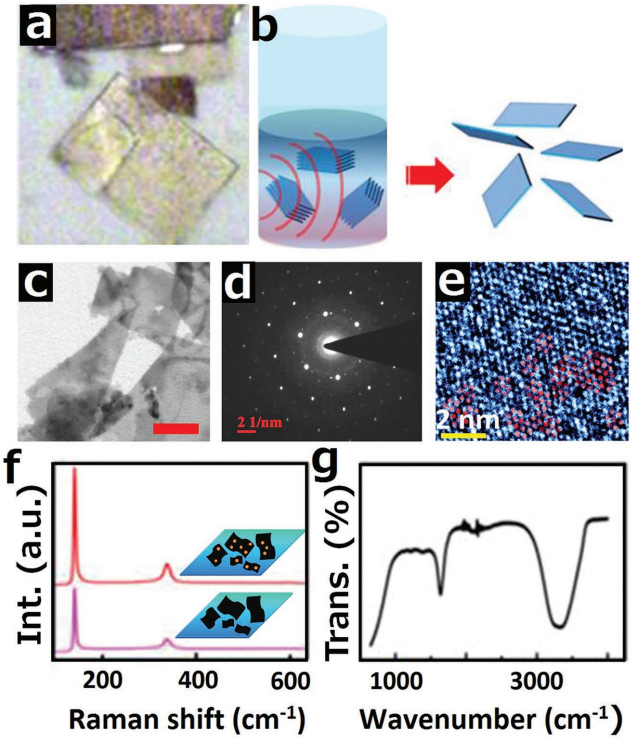

Figure 5. a) Optical image of starting PbO material, b) schematic diagram for sonochemical synthesis, c) TEM image of the sample synthesized in water medium (scale bar is 200 nm), d) SAED pattern taken on a location in (c) and (e) HRTEM image of sample synthesized in water medium (scale bar is 2 nm), f) Raman spectra obtained on PbO sheets without and with Au nanoparticles decorated on it with 633 nm laser, g) FTIR spectrum.

in Figure S7, Supporting Information). Material is crystalline as evidenced by SAED shown in Figure S7b (Supporting Information) and HRTEM image shown in Figure S7c (Supporting Information). Water seems to significantly interact with PbO and its use as a solvent has resulted in large-area atomic sheets as evidenced in the TEM image in Figure 5c. Material synthesized is perfectly crystalline as evidenced by SAED pattern in Figure 5d which shows perfect hexagons. HRTEM image in Figure 5e shows periodic lattice structure in PbO sheets. PbO sheets obtained by sonochemical synthetic route also have been observed to exhibit Raman modes similar to that obtained for PbO by micromechanical method (see Figure 5f). We have utilized decoration of gold nanoparticles to further enhance Raman signals of PbO sheets (see Figure 5f). Fourier transform infrared spectroscopy (FTIR) spectra (see Figure 5g) confirm that there is no presence of trace material other than PbO. Presence of −OH functional group is due to water.

To understand the wettability behavior of PbO surface, piezo inkjet head was used to discharge water droplets at a speed of 1.2 nL s^{-1}. Liquid addition was carried out till droplet volume becomes sufficient enough to monitor the various modes of evaporation. In our case, the overall droplet volume was observed to be 10.8 nL. An inbuilt software (FAMAS) was used to capture snapshots during advancing and receding angles (see **Figure 6**a). It was also used to monitor contact angle (see Figure 6b), droplet height (see Figure 6c), and contact

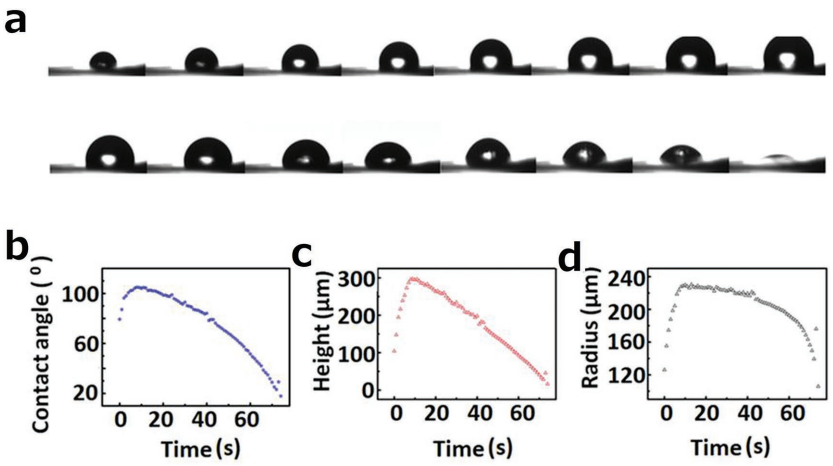

Figure 6. a) Images depicting advancing and receding angles of water droplet on PbO sheet. b) Contact angle, c) contact height, and d) contact radius of the water droplet on PbO sheet, respectively.

radius (see Figure 6d). This software uses half-angle method to measure contact angle. Presence of minor residue after the evaporation confirms that there is no solute particles present in the test fluid. Further to minimize air flow near the substrate holder, the angle meter was positioned far from convective device. These measurements confirm that PbO atomic sheets are hydrophobic in nature with contact angle of 102^0.

Thermogravimetric analysis reveals that MoS_2 sheets actually degrade at elevated temperature above 700 °C. In contrast, PbO shows improved thermal stability as shown in **Figure 7**a. MoS_2 and PbO were tested for microwave stability under household microwave oven (see Figure 7b). Camera images in Figure 7c,d are self-explanatory regarding how enormous damage occurred for MoS_2 and in contrast PbO remained completely unaffected. This observation hints at potential application of PbO atomic sheets as radio wave shielding material for electronic circuits with metallic current lines in mobile phones, laptops, and related devices. To investigate the potential of PbO as anticorrosive coating vis-à-vis MoS_2 as its competing material, we have heated copper sheets without any coating (see camera image in Figure 7e) as well as those coated with MoS_2 (see camera image in Figure 7g) and PbO (see camera image in Figure 7i) on separate sheets in ambient atmosphere at 350 °C for 30 min. Optical imaging of postheat-treated copper sheets with and without coatings establish that PbO coating resist corrosion of copper sheet (see Figure 7j), while MoS_2 coated copper sheet is degraded (see Figure 7h). Resistance of PbO sheets against heating coupled with observed hydrophobicity indicates excellent application of this material for anticorrosion in aqueous atmosphere. As observed in camera images in top and side view for MoS_2 (see Figure 7k,l) and for PbO (see Figure 7m,n), it was found that PbO is resistant to sulfuric acid, while MoS_2 easily dissolves in it. This observation can be useful for potential application of this material for coating on plastic containers for carrying acid, since most of the acid containers (including sulfuric acid) are made up of glass.

In summary, DFT calculations of band structure for α-PbO atomic sheets hint at visible light sensitive PbO atomic sheets which exhibit band gap above 2 eV not only for monolayers, but also for bilayers and trilayers. This input along with thermal stability of material and its low cost hints on its potential applications in phototransistors which can work with visible light. Thus, sensors based on PbO atomic sheets as an active layer, visible light tunability would enhance the electronic signals several orders of magnitude higher, opening up excellent opportunities for chemical/biological molecular sensing. Taking clues from theoretical calculations, we have for the first time demonstrated micromechanical as well as sonochemical exfoliation of α-PbO atomic sheets and propose α-PbO atomic sheets as novel 2D material with band gaps in the visible range in the thickness range from 1 to 30 atomic layers. Various spectroscopic techniques coupled with electron imaging and diffraction establish chemical purity of the 2D crystal. Band gaps of atomic sheets have experimentally been measured and have been found to give a band gap of ≈2 eV (indirect) at three layers and ≈2.2 eV for monolayer. This result is indeed encouraging. Lifetime measurements also indicate layer-dependent fluorescence lifetime which is an interesting result which needs further exploration. We have demonstrated that PbO atomic sheets are hydrophobic in nature and are thermally robust. Potential application as anticorrosive coating has been explored. The material was found to be irresponsive to microwave irradiation even for prolonged duration which indicates its potential in electromagnetic shielding. The novel α-PbO material can also serve as an alternative photonic, optoelectronic, and photovoltaic material, for applications in biosensing, photocatalysis, and energy storage.

Experimental Section

Sample Preparation: Two different strategies were employed for exfoliation of PbO atomic sheets namely micromechanical exfoliation and sonochemical exfoliation. Micromechanical exfoliation was carried out on various substrates namely boro-silicate glass (BSG), n-type Si substrate, and thermally oxidized silicon [SiO_2 (300 nm)/Si]. Sonochemical synthesis was carried out in aqueous phase employing ultrasonicator. The details of the synthesis are described below.

Sample Preparation–Micromechanical Exfoliation: For cleaning BSG substrates, H_2SO_4 + H_2O_2 was used, and then rinsed with ethanol and de-ionized (DI) water thereafter and finally flushed with N_2. Oxidized and unoxidized Si substrates were cleaned by boiling in acetone (@70 °C for 20 min.), rinsed in ethanol and DI water, and then flushed with N_2 jet. First few experiments were carried out to optimize the number of peeling steps needed to achieve atomic sheets. Microscopy experiments were carried out on all the samples with the observation that visibly transparent samples were really thin (below ten layers). Even though there are many factors that determine the thickness of the final transferred sheet on the target substrate (as summarized in Figure S8, Supporting Information), one can roughly estimate that every exfoliation halves the thickness and therefore $t = t_0\ (1/2)^n$. This estimate ignores several important factors and is bound to provide unrealistic estimate; however, when the final number of layers is less, this estimate would be very close. Our initial thickness of the wafer was 20 μm. After ten successive exfoliation steps, the estimated thickness of the flake was found to be ≈20 nm. Upon further exfoliation 11th, 12th, 13th, 14th, and 15th times, it would yield roughly 10, 5, 2.5, 1.2, 0.6 nm, respectively.

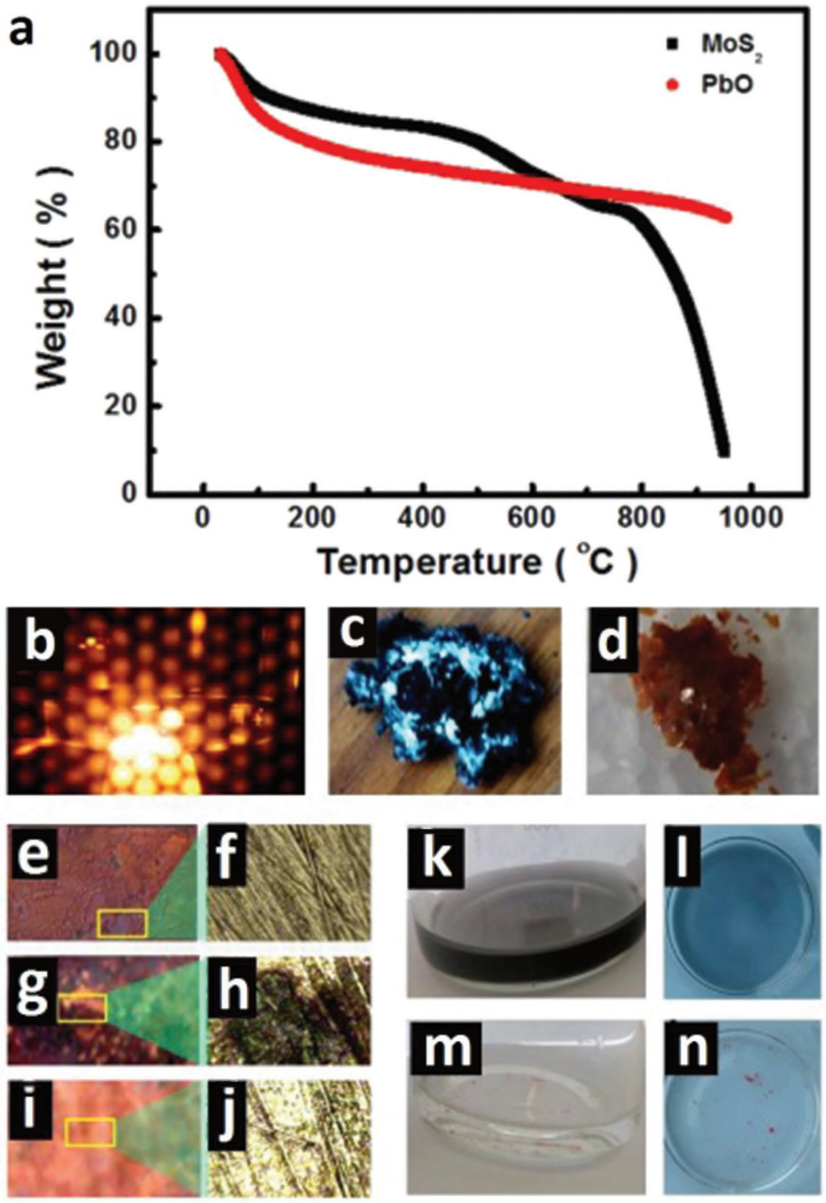

Figure 7. a) Comparative thermogravimetric analysis of MoS_2 and PbO, b) camera image of materials undergoing microwave irradiation, c) camera image of MoS_2, and d) PbO after microwave irradiation. (e) and (f) are camera and optical image of copper sheet without any coating after heating at 350 °C. g) and i) camera image of MoS_2 and PbO coated copper sheets respectively after heating at 350 °C, h,j) optical image of samples in (g) and (i) after ultrasonic cleaning in acetone. k) Side view and l) top view of MoS_2 dispersed in sulfuric acid. m) Side view and n) top view of PbO dispersed in sulfuric acid.

We have, however, validated the estimated thicknesses based on images from atomic force microscopy. Remaining crystal dusts on samples were cleaned by N_2 blower and samples were kept inside vacuum desiccators.

Sample Preparation–Sonochemical Exfoliation: PbO sheets were obtained using sonochemical method in which PbO with equal amounts of 500 mg was taken in two separate beakers and 200 mL of dimethylformamide as well as water solvents were added to each beaker, respectively. The two beakers were inserted in an ultrasonic bath (Cole Parmer, 40 kHz) and the dispersions were ultrasonicated for prolonged duration. Samples were taken out from the sonicating liquid at different times (e.g., 12, 14, 16, 18, and 20 h and so on up to 24 h). The resulting fluid was then centrifuged (Remi, R24) at different rotation speed. It was found that above 6000 rpm, the supernatant contains below ten layers and therefore we used 6000 rpm or higher to attain few layer PbO sheets.

Optical Microscopy and Spectroscopy: Bright and dark-field optical images for samples transferred on transparent BSG substrates were acquired. For optical dark-field imaging, a home-built hyperspectral dark-field imaging microscope was used. The system was built on an Olympus BX51 microscope. A tungsten halogen source (3900, Illumination technologies Inc., East Syracuse, NY) with extremely stable light output (0.1%) was coupled to a CytoViva dark-field condenser (N.A 1.2–1.4) via a fiber optic light guide. Prealigned Koehler illumination let the tungsten halogen source focus on the entrance slit of the condenser. The scattering light was collected with a 100x oil objective with an iris, then split into two light paths, one is for direct optical dark-field imaging and the other for spectra measurements. The scattering light illuminates the narrow slit of the spectrograph to generate 1D image. The 1D image was dispersed by the grating in the spectrograph and then collected by the thermoelectrically cooled (air) charge coupled device (CCD) (PIXIS-400BR, Princeton Instruments).[41] Spectra were recorded from 400 to 900 nm in the entire region of interest with 0.3 s exposure time and the averaged data were presented.

FESEM and AFM: FESEM (FEI Inc., working at 20 kV) and atomic force microscopy (VEECO Inc., working in dynamic force mode) were used to characterize the microstructures of the samples transferred on Si substrates.

TEM: JEOL 2100 was used to acquire TEM/HRTEM images and for SAED. PbO dispersion was used for thin coating on carbon-coated copper grid for microscopy purpose.

Photoluminescence Microscopy and Spectroscopy: The PL measurement of the PbO atomic crystals was performed with the Zeiss LSM 710 scanning confocal microscopy (Zeiss, Germany). Samples were excited by the 488 nm laser line. PL emissions from PbO sheets were spatially filtered by a 100 µm pinhole and spectrally filtered by long pass filters before being recorded in a 34-channel QUASAR detection unit in the LSM 710. PL images were collected simultaneously. The spectrum of PbO under 488 nm laser line excitation was constructed by quantifying PL intensities at different wavelength, and the spectrally coded PL image was reconstructed accordingly with the Zeiss Zen software. Florescence lifetime imaging measurements were also carried out on PbO sheets.

Raman Spectroscopy: Raman spectra were recorded within the wave number range 88–400 cm^{-1} in the back scattering geometry using confocal Micro-Raman Spectrometer (Seki Technotron Corporation, Japan) with 514 nm Argon ion LASER as excitation source by STR Raman Spectrograph. A 100X microscope was used to focus the LASER beam and collect the light.

X-Ray Photoelectron Spectroscopy: Kratos AXIS Ultra DLD Imaging XPS was used for evaluating valency states of PbO. XPS was done in ultra high vacuum (UHV) conditions on solid phase.

X-Ray Diffraction: For the phase purity and structural analysis sample, XRD patterns were recorded using an X-ray diffractometer (Rigaku TTRX III diffractometer) with Cu Kα (1.542 Å) radiation.

Thermogravimetric Analysis: Thermogravimetric measurement was done 30–950 °C at rate of heating 10 °C min^{-1} to confirm the phase stability of PbO at high temperature in a Perkin Elmer Instrument.

Contact Angle Measurements: Contact angle measurements were performed by Kyowa Interface Science MCA-3, an automatic contact angle meter. A temperature of 27 °C and relative humidity of 56% were recorded using temperature and humidity sensor at the time of measurement, which were mounted at the backside of the substrate. Double distilled Millipore water was used for all measurement.

Computation Details: α-PbO crystal structure was obtained from AMCSD.[42] Unit cell of α-PbO monolayer consists of two Pb and two oxygen atoms. With an increase in the number of layers, number of atoms per unit cell multiplies by four. Thus, for an eight-layered system, there are a total of 32 atoms in the unit cell. All of the calculations were performed using DFT with PBE exchange correlation functional and with plane-wave basis set as implemented in the Quantum ESPRESSO package. Ultrasoft pseudopotentials, Pb.pbe-dn-rrkjus_psl.0.2.2.UPF and O.pbe-n-rrkjus_psl.0.1.UPF, with nonlinear core corrections, were considered for both Pb and O atoms, respectively, from http://www.quantum-espresso.org/.[43] The reported results are accurate to 0.001 Ry and the converged parameters for kinetic energy cutoff, charge density cutoff, k-mesh, degauss, and vacuum are 80 Ry, 640 Ry, $8 \times 8 \times 8$, 0.02 Ry, and 12 Å, respectively. Van der Waals interactions among the layers of PbO were accounted for through Grimme's DFT-D correction.[44] Systems are considered to be relaxed when the forces on the atoms are less than 0.001 Ry per Bohr.

Supporting Information

Supporting Information is available from the Wiley Online Library or from the author.

Acknowledgements

J.L. and P.R. contributed equally to this work. Financial assistance in the form of National Research Council Senior Research Associateship (G.J.C.), and NSF Grant Nos. CMMI-0547636 and CMMI 0928752 (G.J.C.) has been crucial for these experiments. P.K. acknowledges financial support from Science and Engineering Research Board, Department of Science and Technology, Government of India in the form of The Ramanujan Fellowship (sanction no. SB/S2/RJN-205/2014). S.R.K.C.Y. thanks TUE-CMS for computational facilities. X.W. is acknowledged for assistance in dark-field imaging. G.J.C. and P.K. conceived the idea. P.K., Y.H. carried out micromechanical exfoliation and P.R. carried out sonochemical synthesis of PbO atomic sheets. J.I. and J.L. discussed lifetime approaches to material characterization and J.L. carried out PL imaging and analysis. S.R.K.C.Y. carried out band structure calculations under supervision of S.K.P. and P.K. wrote the paper and incorporated feedback from all the authors. Finally, J.I. and G.J.C. reviewed and revised the manuscript.

Conflict of Interest

The authors declare no conflict of interest.

Keywords

band structure calculation, lead oxide atomic sheets, photoluminescence

Received: September 26, 2017
Revised: December 17, 2017
Published online: February 12, 2018

[1] K. S. Novoselov, A. K. Geim, S. V. Morozov, D. Jiang, Y. Zhang, S. V. Dubonos, I. V. Grigorieva, A. A. Firsov, *Science* **2004**, *306*, 666.
[2] A. K. Geim, K. S. Novoselov, *Nat. Mater.* **2007**, *6*, 183.
[3] S. Bae, H. Kim, Y. Lee, X. Xu, J. S. Park, *Nat. Nanotechnol.* **2010**, *5*, 574.
[4] F. Bonaccorso, Z. Sun, T. Hasan, A. C. Ferrari, *Nat. Photonics* **2010**, *4*, 611.
[5] J. Liu, P. Kumar, Y. Hu, G. J. Cheng, J. M. Irudayaraj, *J. Phys. Chem. C* **2015**, *119*, 6331.
[6] P. Kumar, *RSC Adv.* **2013**, *3*, 11987.
[7] P. Kumar, L. S. Panchakarla, C. N. R Rao, *Nanoscale* **2011**, *3*, 2127.
[8] P. Kumar, S. S. R. K. C. Yamijala, S. K. Pati, *J. Phys. Chem. C* **2016**, *120*, 16985.
[9] K. S. Novoselov, V. I. Fal'ko, L. Colombo, P. R. Gellert, M. G. Schwab, K. Kim, *Nature* **2012**, *490*, 192.
[10] A. Splendiani, L. Sun, Y. Zhang, T. Li, J. Kim, C. Y. Chim, G. Galli, F. Wang, *Nano Lett.* **2010**,*10*, 1271.
[11] G. Eda, H. Yamaguchi, D. Voiry, T. Fujita, M. Chen, M. Chhowalla, *Nano Lett.* **2011**, *11*, 5111.
[12] B. Radisavljevic, A. Radenovic, J. Brivio, V. Giacometti, A. Kis, *Nat. Nanotechnol.* **2011**, *6*, 147.
[13] O. L. Sanchez, D. Lembke, M. Kayci, A. Radenovic, A. Kis, *Nat. Nanotechnol.* **2013**, *8*, 497.
[14] T. Jiang, H. Liu, D. Huang, S. Zhang, Y. Li, X. Gong, Y. R. Shen, W. T. Liu, S. Wu, *Nat. Nanotechnol.* **2014**, *9*, 825.
[15] K. Liu, L. Zhang, T. Cao, C. Jin, D. Qiu, Q. Zhou, A. Zettl, P. Yang, S. G. Louie, F. Wang, *Nat. Commun.* **2014**, *5*, 4966.
[16] R. S. Sundaram, M. Engel, A. Lombardo, R. Krupke, A. C. Ferrari, P. Avouris, M. Steiner, *Nano Lett.* **2013**, *13*, 1416.
[17] Z. He, Y. Sheng, Y. Rong, G. D. Lee, J. Li, J. H. Warner, *ACS Nano* **2015**, *9*, 2740.
[18] R. Coehoorn, C. Haas, R. A. Groot, *Phys. Rev. B* **1987**, *35*, 6203.
[19] H. J. Conley, B. Wang, J. I. Ziegler, R. F. Haglund Jr. , S. T. Pantelides, K. I. Bolotin, *Nano Lett.* **2013**, *13*, 3626.
[20] J. Mann, Q. Ma, P. M. Odenthal, M. Isarraraz, D. Le, E. Preciado, D. Barroso, D. Yamaguchi, G. V. S. Palacio, A. Nguyen, T. Tran, M. Wurch, A. Nguyen, V. Klee, S. Bobek, D. Sun, T. F. Heinz, T. S. Rahman, R. Kawakami, L. Bartels, *Adv. Mater.* **2014**, *26*, 1399.
[21] Y. Gong, J. Lin, X. Wang, G. Shi, S. Lei, Z. Lin, X. Zou, G. Ye, R. Vajtai, B. I. Yakobson, H. Terrones, M. Terrones, B. K. Tay, J. Lou, *Nat. Mater.* **2014**, *13*, 1135.
[22] K. Roy, M. Padmanabhan, S. Goswami, T. P. Sai, G. Ramalingam, S. Raghavan, A. Ghosh, *Nat. Nanotechnol.* **2013**, *8*, 826.
[23] P. Miro, M. Audiffred, T. Heine, *Chem. Soc. Rev.* **2014**, *43*, 6537.
[24] S. Lebegue, T. Bjorkman, M. Klintenberg, R. M. Nieminen, O. Eriksson, *Phys. Rev. X* **2013**, *3*, 031002.
[25] G. Trinquiert, R. Hoffmann, *J. Phys. Chem.* **1984**,*88*, 6696.
[26] L. Heijne, P. Schagen, H. Bruining, *Nature* **1954**, *173*, 220.
[27] J. Leciejewicz, *Acta Crystallogr.* **1961**, *14*, 1304.
[28] P. Canepa, P. Ugliengo, M. Alfredsson, *J. Phys. Chem. C* **2012**, *116*, 21514.
[29] J. Berashevich, O. Semeniuk, J. A. Rowlands, A. Reznik, *Europhys. Lett.* **2012**, *99*, 47005.
[30] D. Adams, D. Stevens, *Dalton Trans.* **1976**, *371*, 1096.
[31] H. Wang, C. Zhang, F. Rana, *Nano Lett.* **2015**,*15*, 8204.
[32] Y. Wang, X. Lin, H. Zhang, T. Wen, F. Huang, G. Li, Y. Wang, F. Liao, J. Lin, *CrystEngComm* **2013**, *15*, 3513.
[33] Y. Cui, X. Wang, W. Ren, J. Liu, J. Irudayaraj, *ACS Nano* **2016**,*10*, 3132.
[34] S. Rondon, P. M. A. Sherwood, *Surf. Sci. Spectra* **1998**, *5*, 90.
[35] F. Hu, Z. Cao, C. Zhang, X. Wang, M. Xiao, *Sci. Rep.* **2015**, *5*, 8898.

[36] K. Hao, G. Moody, F. Wu, C. K. Dass, L. Xu, C. H. Chen, L. Sun, M. Y. Li, L. J. Li, A. H. MacDonald, X. Li, *Nat. Phys.* **2016**, *12*, 677.
[37] L. Yang, N. A. Sinitsyn, W. Chen, J. Yuan, J. Zhang, J. Lou, S. A. Crooker, *Nat. Phys.* **2015**,*11*, 830.
[38] A. Srivastava, M. Sidler, A. V. Allain, D. S. Lembke, A. Kis, A. Imamoğlu, *Nat. Nanotechnol.* **2015**, *10*, 491.
[39] D. Lagarde, L. Bouet, X. Marie, C. R. Zhu, B. L. Liu, T. Amand, P. H. Tan, B. Urbaszek, *Phys. Rev. Lett.* **2014**, *112*, 047401.
[40] Z. Guo, H. Zhang, S. Lu, Z. Wang, S. Tang, J. Shao, Z. Sun, H. Xie, H. Wang, X. F. Yu, P. K. Chu, *Adv. Funct. Mater.* **2015**, *25*, 6996.
[41] S. C. Dhanabalan, J. S. Ponraj, Z. Guo, S. Li, Q. Bao, H. Zhang, *Adv. Sci.* **2017**, *4*, 1600305.
[42] R-Ruff, *American Minerologist Crystal Structure Database*, http://rruff.geo.arizona.edu/AMS/amcsd.php (accessed: Aug **2015**).
[43] P. Giannozzi, S. Baroni, N. Bonini, M. Calandra, R. Car, C. Cavazzoni, D. Ceresoli, G. L. Chiarotti, M. Cococcioni, I. Dabo, A. D. Corso, S. d. Gironcoli, S. Fabris, G. Fratesi, R. Gebauer, U. Gerstmann, C. Gougoussis, A. Kokalj, M. Lazzeri, L. M. Samos, N. Marzari, F. Mauri, R. Mazzarello, S. Paolini, A. Pasquarello, L. Paulatto, C. Sbraccia, S. Scandolo, G. Sclauzero, A. P. Seitsonen, A. Smogunov, P. Umari, R. M. Wentzcovitch, *J. Phys. Condens. Matter* **2009**, *21*, 39.
[44] S. Grimme, J. Antony, S. Ehrlich, H. A. Krieg, *J. Chem. Phys.* **2010**, *132*, 154104.

